RESEARCH ARTICLE

VOLCANICA

Submitted: 2023-02-08 | Accepted: 2023-07-12 | Published: 2023-08-24

# Experimental insights into factors influencing Vp/Vs ratios at the Nevado del Ruiz Volcano, Colombia

Joaquin Pablo Aguilera Bustos*[α] and Ludmila Adam[α]

[α] School of Environment, Faculty of Science, Science Centre, The University of Auckland, 23 Symonds St, Auckland, New Zealand.

## Abstract

Measurements of ultrasonic elastic waves on lithologies that form the Nevado del Ruiz Volcano (NRV) were carried out at atmospheric and in-situ pressure conditions. The study focuses on P- and S-wave velocity ratios "*Vp/Vs*" as a function of *Vp* as indicators of mineralogy, porosity, fluid-types and anisotropy. Rock samples were collected from outcrops and the well Nereidas-1 which include altered and unaltered volcanic and metamorphic rocks (andesites, andesitic tuff, greenschists, and meta-sandstones). Changes in *Vp/Vs* are commonly interpreted in seismic tomography studies in volcanic and geothermal areas as being due to fluid changes. The bulk modulus of the fluid influences the *Vp/Vs*, the stiffer the fluid (e.g. magma) the higher the *Vp/Vs* ratio. In addition, our study outlines that other rock and subsurface parameters can also significantly influence such ratios. We find that *Vp/Vs* ratios can separate the effect of microcracks vs. vesicles as a function of fluid type and effective pressures. Little-to-no pressure dependence in *Vp/Vs* suggest that the rock porosity is mainly comprised of vesicles, while largely varying *Vp/Vs* vs *Vp* is associated with cracks. This effect occurs under both dry and fluid saturated conditions. When cracks close, the *Vp/Vs* values are representative of the rock mineralogy. Finally, elastic waves anisotropy due to foliation results in a wide range of *Vp/Vs* ratios, which could lead to misinterpretation. For instance, in the NRV foliated rocks, *Vp/Vs* at dry conditions and parallel to the foliation plane are the same as those commonly associated to fluid saturation.

Keywords: Vp/Vs; Foliation; Andesites; Metamorphic; Fluids; Geothermal.

## 1 Introduction

The P- to S-wave velocity ratio (*Vp/Vs*) is a commonly used tool for seismic subsurface characterization due to its sensitivity to changes in rock and fluid physical properties such as porosity and structural composition [O'Connell and Budiansky 1974; Boitnott and Kirkpatrick 1997; Peacock et al. 2011; Wang et al. 2012; Amalokwu et al. 2016; Ding et al. 2019; Fliedner and French 2021], mineralogy and rock lithology [Tatham 1982; Castagna et al. 1985; Wang 2001; Wilkens et al. 2018], fluid types [Castagna and Backus 1993; Brantut and David 2018], and effective stress [Romero-Jr et al. 1995; Peacock et al. 2011; Markus et al. 2022]. This sensitivity is due to the P- and S-wave speed responding differently to the rock and fluid properties.

Both P- (*Vp*) and S-wave (*Vs*) velocities are sensitive to fluids, but their sensitivity varies. For *Vp*, the bulk modulus sensitivity to fluids is commonly more significant than that for the density; for *Vs* the sensitivity to fluids comes uniquely from the density effect. Isotropic wave speeds are defined as the ratio between the rock elastic moduli and its density. P-waves depend on the bulk ($K$), which defined the elastic response to hydrostatic compressional stresses, and shear moduli. The shear modulus ($G$) defines the elastic response to shear stresses. $G$ is insensitive to fluids in the pore space, meaning that the shear modulus is constant whether the rock is dry or water-saturated [Lowrie and Fichtner 2020]. In contrast, the bulk modulus is highly sensitive to the compressibility of the fluid in the pore space, allowing it to be a fluid discriminator [Batzle and Wang 1992; Castagna and Backus 1993; Wang 2001].

By taking the *Vp/Vs* ratio, the influence of density is eliminated and the ratio only depends on the rock elastic moduli:

$$\frac{Vp}{Vs} = \frac{K}{G} + \frac{4}{3}. \tag{1}$$

In a volcanic setting, a high *Vp/Vs* is usually interpreted as magma (melt) or water-saturated rocks [Nakajima et al. 2001a; b; Koulakov et al. 2009; Peacock et al. 2011; Londono and Kumagai 2018]. Low *Vp/Vs* is associated with the presence of dry steam or gas phases [Boitnott and Kirkpatrick 1997; Chiarabba and Moretti 2006; Delliansyah et al. 2015]. This interpretation is based on the fact that the shear modulus is insensitive to the pore saturating fluid, while the bulk modulus is highly sensitive to fluid type [Batzle and Wang 1992; Castagna and Backus 1993; Wang 2001]. The more incompressible the fluid is, the higher the bulk modulus and thus the *Vp/Vs* ratio. Fluid overpressure can also increase Vp/Vs ratios significantly as observed in subduction zones [Peacock et al. 2011; Pimienta et al. 2018].

The *Vp/Vs* ratio is commonly interpreted in conjuction with *Vp*. The analysis of *Vp/Vs* vs. *Vp* can be used as a lithology discriminator. For instance, *Vp/Vs* allows the discrimination between sandstones, carbonates and shales [Tatham 1982; Wang 2001]. Wilkens et al. [2018] shows that carbonate content controls *Vp/Vs* in siliceous limestones.*Vp/Vs* also depends on other physical rock properties such a porosity and pore shape. This occurs not only in sedimentary rocks but has also been explored and quantified on volcanic and metamorphic rocks at in-situ depth conditions (effective stress and presence of fluids) [Tatham 1982; Boitnott 1995; Pimienta et al. 2018; Fliedner and French 2021].

* pablo.aguilera@auckland.ac.nz

Editor: A. R. L. Kushnir | Typesetter: J. Farquharson

Seismic tomographic images of *Vp/Vs* in volcanic and geothermal environments have been created in 3D [Koulakov et al. 2009; Londono 2010; Gritto et al. 2013] as well as a function of time [Patanè et al. 2006; Gritto and Jarpe 2014; Vargas et al. 2017; Zhu 2018]. Although this ratio is central to the interpretation of rock physical properties [Boitnott and Kirkpatrick 1997; Lin et al. 2015] most interpretations of Vp/Vs lean towards the interpretation of the presence of fluids. [Nakajima et al. 2001a; b; Kasatkina et al. 2014; Vargas et al. 2017; Londono and Kumagai 2018]. In this study we show the influence of a range of rock and fluid parameters on *Vp/Vs* for a volcanic and geothermal region in Colombia: the Nevado del Ruiz volcano.

Seismic tomography analysis provides *Vp/Vs* ratios with depth, which to date have been interpreted mostly in terms of magma and gas flows as part of the active hydrothermal systems in volcanic areas [Londono 2010; Vargas et al. 2017; Londono and Kumagai 2018]. However, there are other rock physical properties or subsurface conditions that can influence the *Vp/Vs* ratios in a volcanic area. The simplistic interpretation of seismic tomography data to-date is due to the lack of borehole and laboratory wave speed data. Here we combine laboratory experiments and numerical modeling on core collected at the NRV to present alternative physical properties and reservoir conditions which control the *Vp/Vs* ratio at the NRV. We measure ultrasonic P- and S-wave velocities for dry and water-saturated rocks at variable effective pressure conditions. Specifically, we investigate how porosity, pore geometry, fluids, foliation, effective pressure, and mineralogy influence *Vp/Vs* in key lithologies that comprise the NRV.

## 2 Geological setting and core sampling at the NRV

The NRV is a stratovolcano located in the Central Cordillera of Colombia near the city of Manizales and about 150 km west of the Colombian capital city Bogotá. The volcano has an active hydrothermal system and a prospective geothermal area to the west of it [Monsalve et al. 1998; González-García et al. 2015; Moreno et al. 2018; Vélez et al. 2018] (Figure 1). This stratovolcano has been built by different eruptive events during the Quaternary period that have deposited andesite lavas over a metamorphic basement and intrusive rocks [Ceballos-Hernandez et al. 2020]. Four main eruptive periods have been identified for the NRV: The Pre–Ruiz eruptive period (PRE) dominated by effusive volcanism from 1.8 to 0.97 Ma; the First eruptive period Ruiz (FEPR) defined by effusive volcanism before 0.97 Ma, ending with the construction of La Olleta (OLL) Volcano at approximately 107 ka; the destructive period of the "Older Ruiz" volcano at ~95 ka; the Intermediate eruptive period Ruiz continued construction of OLL and was the origin of other volcanoes and minor eruptive centers; and the Second eruptive period Ruiz (SEPR) that began 66 ka ago. For the last 13 ka, the NRV has experienced explosive activities with at least fourteen pulses and eruptive phases that include lava formations (LAV) and welded andesitic tuff or ignimbrites (IGN). As mentioned, these volcanic products overlie a metamorphic basement known as the Cajamarca Group associated with Permian-Late Jurassic metamorphism [Tapias et al. 2017]. These andesites also overly some intrusive bodies dating to the Eocene period such as the formation known as the Manizales Stocks (MS) [Ceballos-Hernandez et al. 2020].

The stratigraphy from the only exploratory geothermal well in the NRV (Nereidas-1) agrees with the field stratigraphy described above [Monsalve et al. 1998]. The well stratigraphy shows metamorphic rocks as basement overlaid by andesite rocks. Therefore, we carried out the core field sampling based on both the information from the Nereidas-1 well and the surface geological maps of the NRV volcanic units [Ceballos-Hernandez et al. 2020] as shown in Figure 1.

A total of ten locations around the NRV were sampled. Sampling sites were selected by a field geologist from the Colombian Geological Survey, which corresponded to key localities representing each of the formations that compose the NRV. If observed, hydrothermal alteration at those localities was also sampled, but there was no consistent sampling of hydrothermal alteration due to the lack of exposed rocks. The large samples were sub-cored to 14 cylinders, 25 mm in diameter. Additionally, two cores were extracted from borehole core from the Nereidas-1 well at a depth of 1225 m, one sample containing a quartz vein (NV) and the other core sampling the rock matrix (NM). Because the Cajamarca Group is formed by foliated metamorphic rocks, two cores perpendicular to each other and visually aligned with the foliation were sampled for the metasandstones (Meta) and schists lithologies. Figure 2 summarizes the stratigraphic units at the NRV with the corresponding images of rock samples collected from field outcrops and the Nereidas-1 well (only one sample for Meta and Schist are shown in the Figure). Therefore, a total of 16 cores were analysed.

## 3 Sample preparation and experimental methods

Porosity was measured at atmospheric conditions with a Vinci Technologies nitrogen gas porosimeter [Duran et al. 2019b]. The values obtained for each sample are specified in Table 1. XRD analysis was performed by Panda Geosciences for each rock sample using the Philips 1130 XRD machine. Additionally, mineral interpretation were carried out using a Nikon LV100 Pol microscope with digital camera. Sample mineralogies are summarised in Table 1 and in Supplementary Material 1.

The rock samples show variable mineralogy with some samples showing hydrothermal alteration. For instance, the silica minerals cristobalite and tridymite, found in samples PRE-2, PRE-3, and SEPR, and proximal to faults, are the result of devitrification and hydrothermal alteration [Getahun et al. 1996; Baxter et al. 1999; Murphy et al. 2000; de Hoog et al. 2019] (Figure 1). Also, at the sector where PRE-2 and PRE-3 were sampled, previous studies have found the presence of an advanced argillic hydrothermal alteration [Forero et al. 2011]. The presence of illite in sample PRE-2 points such alteration. PRE-1 is associated with the same geological formation as PRE-2 and PRE-3, showing similar mineralogy. However, this sample was collected from an outcrop with no evidence of hydrothermal alteration and contain smectite, which is possibly caused by weathering [Wilson 2004; Schulze 2005]. The

6(2): 283–299. https://doi.org/10.30909/vol.06.02.283299

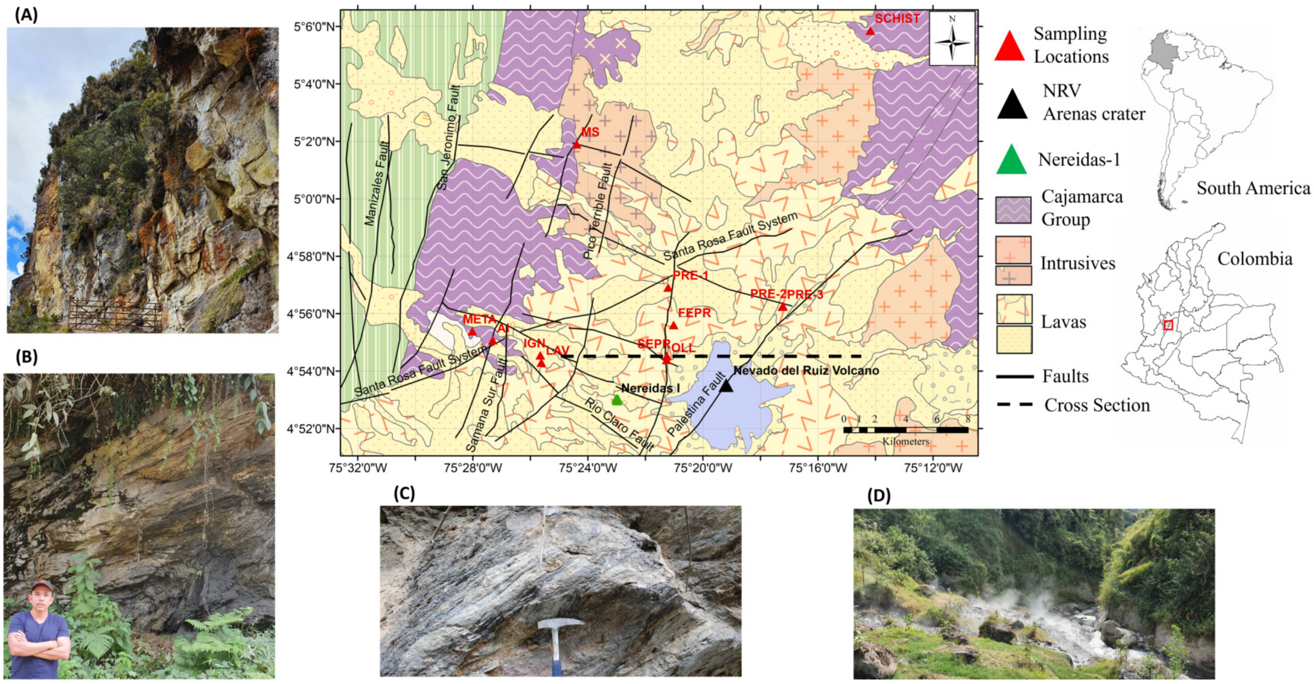


Figure 1: Geological map of the study area modified from González-García et al. [2015] and outcrop pictures of some of the main sampling sites. The map shows the location of the NRV (black triangle), faults (solid lines), rock sampling locations (red triangles) and location of well Nereidas-1 (green triangle). The labels of the rock sampling locations are associated with the geological formations as follow PRE-1, PRE-2, and PRE-3 ([A] at the convergence between Santa Rosa fault System and Palestina Fault) are associated with the Pre-Ruiz Eruptive Period (PRE); FEPR with First Eruptive Period Ruiz; OLL with the Olleta crater formation; SEPR with Second Eruptive Period Ruiz; samples LAV and IGN are also related to the Second Eruptive Period Ruiz; MS (Manizales Stock) and AI (unidentified altered intrusive) with intrusive bodies; and Schist [B] and META (Metasandstone, [C]) are rock formations from the Cajamarca Group. [D] is a discharge zone of the geothermal field at the converge between Santa Rosa Fault System and Samaná Sur Fault. The right inset map shows the study area location (red square). GCS-WGS Geographic Coordinate System_World Geodetic System.

rest of the samples associated with the NRV eruption periods FEPR, IEPR and SEPR have similar composition to PRE-1. They are andesites mainly comprised of plagioclase, augite, and volcanic glass including the andesitic tuff labeled as IGN. Samples NM and NV from the well Nereidas-1 are described by Monsalve et al. [1998] as calcsilicate gneiss. The microphotographs and XRD analysis suggest that these samples are garnet skarns. Due to the presence of epidote, sericite, and calcite as secondary minerals, Monsalve et al. [1998] defines the lithological horizon from where NM and NV were extracted as thermometamorphic associated with propylitic alteration. The mineralogy of sample AI points to hydrothermal alteration as it contains chlorite, illite, and apatetite. This sample was collected from a sector identified as the discharge zone of the NRV geothermal system known as Botero-Londono [González-García et al. 2015; Vélez et al. 2018]. The sample MS is identified as an intrusive quartz monzodiorite with minerals such as biotite, quartz, and plagioclase. This rock composition confirms that we effectively sampled the intrusive volcanic formation known as The Manizales Stock, which has been described having quartz dioritic–tonalitic composition [Ceballos-Hernandez et al. 2020].

P- and S-waves were measured for dry and water-saturated samples using a pair of ultrasonic transducers at the atmospheric pressure (central frequency of 0.5 MHz) and at confining pressures between 3.4 and 69.4 MPa (central frequency of 1 MHz, more information on the setup can be found in Supplementary Material 2). At atmospheric pressures, two pairs of transducers are used: P-wave and S-wave transducers. For the waveforms acquired under confining pressure, one pair of transducers is attached to the top and bottom of the sample (Supplementary Material 2). Inside each of these high-pressure transducers are three crystals that generate one P-wave and two orthogonal S-waves. An electronic switch box is used to change between crystals. Two hundred and fifthy six waveforms are averaged for each experimental measurement to reduce random noise. To saturate the samples we fist vacuum the samples to remove any air and then inject water via two fluid lines at the top and bottom of the sample at a constant fluid pressure of 3.4 MPa while the confining pressure was 6.8 MPa. When no more fluid flow is measured in the fluid pump, we assume that the sample is saturated. The fluid pressure remains constant throughout the experiment. Only the

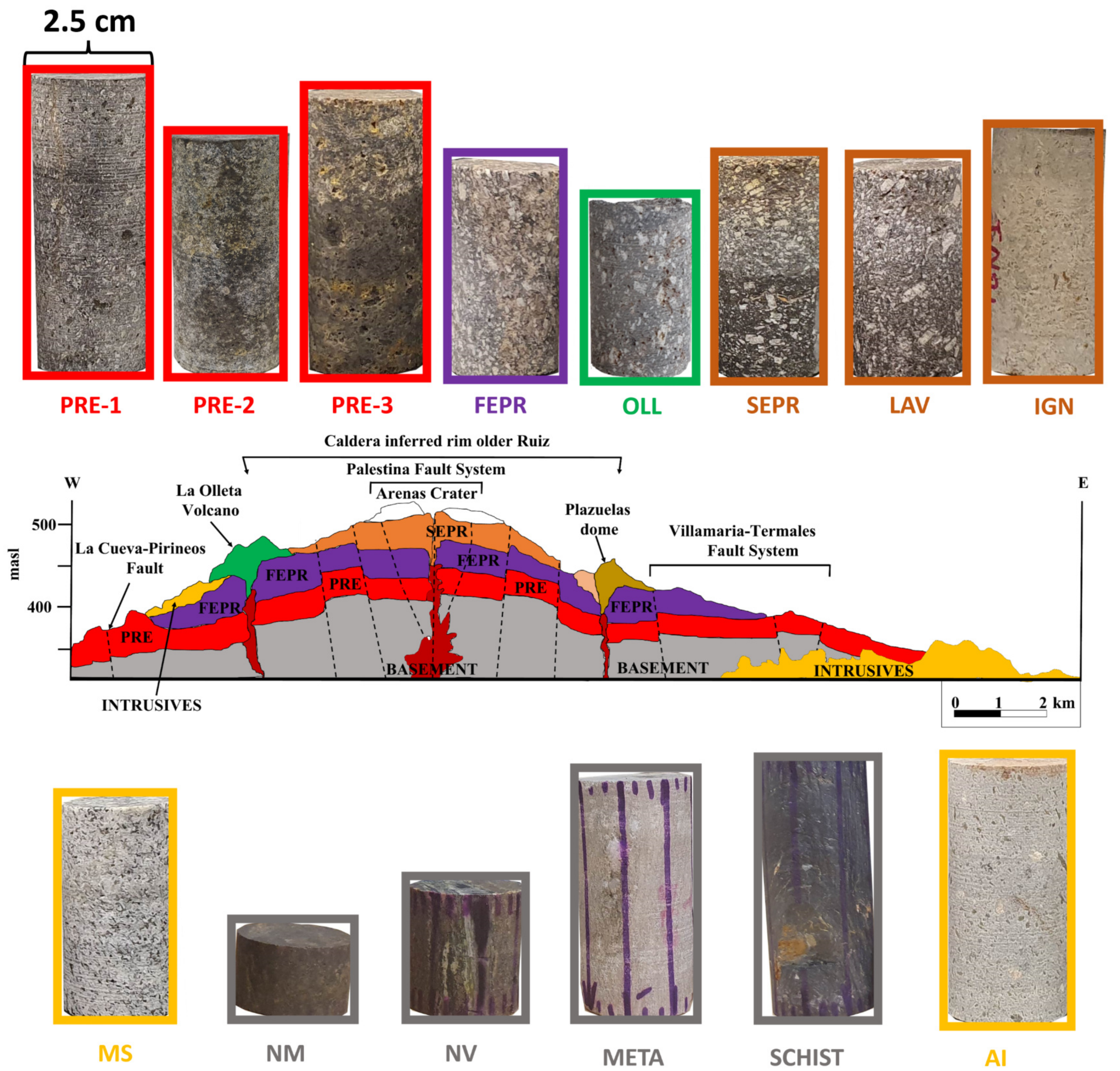


Figure 2: The NRV general stratigraphy (cross section from Figure 1) with the corresponding rock samples in this study. All samples, other than the Nereidas-1 samples are collected from outcrops. Volcanic units from the NRV are sampled for the different the NRV eruptive periods and the rock samples AI and MS are associated with intrusive formations. The basement rocks are from the metamorphic formation Cajamarca Group. The outline color of each sample indicates the respective geological formation in the cross-section. The cross-section (location indicated by the dashed line from Figure 1) is modified from Ceballos-Hernandez et al. [2020]. For scale purpose, the diameter of each cylinder is 2.5 cm.

connected porosity of the samples will be saturated with water, any unconnected porosity would remain dry. Given that the samples have significant volumes of microcracks, we believe the samples are saturated close to or at full saturation. Confining pressures are then varied from 6.8 to 69.4 MPa. For anisotropic samples, rotational measurements at room conditions were performed to identify the foliation plane as a guide for the transducer alignment for measurements under confining pressure.

First arrival times were estimated using the dynamic time-warping algorithm by Duran et al. [2019a]. Velocities and associated standard deviations are estimated from the time and length measurements, and their errors. Figure 3 show examples of P- and S-wave waveforms for sample SEPR under effective pressures from 3.3 to 66.0 MPa. Associated P- and S-wave arrival times are displayed on the waveforms.

Table 1: Porosity, mineral and lithology identification from XRD and microphotographs. Mineral abbreviations: Ab: Albite, Add: Andradite, Amp: Unidentified amphibole, Ap: Apatite, Aug: Augite, Bt: Biotite, Cal: Calcite, Chl: Chlorite, Cpx: Clinopyroxene, Crs: Cristobalite, Ep: Epidote, Fsp: Unidentified feldspar, Gt: Garnet, Hb: Hornblende, I: Illite, Kfs: K–feldspar, Opq: Unidentified opaque, Pl: Plagioclase, Q: Quartz, Sm: Smectite, Trd: Tridymite, Tt: Titanite. Porosities are at atmospheric pressures.

| Unit | Sample | Porosity (%) | XRD-Minerals | | | Petrographical interpretation | Description |
|---|---|---|---|---|---|---|---|
| | | | Major | Minor | Trace | | |
| SEPR | IGN | 27.60 ± 0.54 | Pl, Aug | | | Pl, Cpx, glass, Opq | Andesite tuff |
| | LAV | 11.64 ± 0.06 | Pl, Aug | Crs | I/Mica | Pl, Cpx, glass, Opq, Hb | Andesite |
| | SEPR | 7.14 ± 0.08 | Pl, Aug | | | Pl, Aug, Opq, Hb, glass | Andesite |
| IEPR | OLL | 10.87 ± 0.04 | Pl, Aug | Amp | | Pl, Aug, Opq, Hb, glass | Andesite |
| FEPR | FEPR | 9.39 ± 0.01 | Pl, Aug | Trd, Crs | | Pl, Aug, Opq, glass | Andesite |
| PRE | PRE-1 | 1.36 ± 0.04 | Pl | Aug, Sm | I/Mica, Q | Pl, Cpx, Opq, SM, Q, Hb | Altered Andesite with Q vein |
| | PRE-2 | 2.71 ± 0.23 | Pl, Aug | Trd, Crs | I/Mica | Pl, Aug, Opq, Bt | Andesite |
| | PRE-3 | 8.04 ± 0.11 | Pl, Trd, Crs | Aug | | Pl, Cpx, Crs, Trd, Hb, Opq, Q | Altered Andesite with Q xenoliths |
| INTRUSIVES | MS | 1.99 ± 0.04 | Pl, Mica | Aug, Q | Chl | Pl, Q, Bt, Kfs,Ep, Tt, Ap, Opq | Quartz monzodiorite |
| | AI | 1.48 ± 0.09 | Q, Pl, Chl, I | Cal | | Chl, I, Q, Pl, Opq, Ap | Altered Andesite |
| CAJAMARCA GROUP | Meta | 10.36 ± 0.09 | Chl, Q | Pl | | Q, Chl, Kfs, Ab | Meta-sandstone |
| | Schist | 12.94 ± 0.07 | Chl, Mica, Q | | | Chl, Mica, Q, Ep | Greenschist |
| NEREIDAS-1 | NM | 2.69 ± 0.11 | Add | Q | Chl | Gt, Ep, Q, Amp, Opq | Garnet-Skarn |
| | NV | 1.50 ± 0.17 | Add, Q | Pl, Kfs | Chl | Gt, Ep, Q, Opq, Fsp | Greenschist |

## 4 Numerical modeling

When rocks are subjected to increasing effective pressures, the shape of the pores plays a role in varying the ultrasonic elastic velocities [O'Connell and Budiansky 1974]. The shape of the pore can be described by the aspect ratio (α), which defines the ratio between the short and long axis of a two- or three-dimensional ellipse [Wang 2001]. The aspect ratio is always less than or equal to one. Very low aspect ratios ($\alpha \ll 1$) are used to describe cracks and their density and shape are associated with them opening/closing as a result of variable effective pressures [Walsh 1965]. A high aspect ratio ($\alpha \approx 1$) is related to vesicles or vugs and describe pressure independent porosity [Wang et al. 2015; Duran et al. 2019b].

We use the Kuster and Toksöz (KT) model [Kuster and Toksöz 1974] to estimate the effective bulk $K_{KT}$ and shear $\mu_{KT}$ moduli as a sum of volumetric contributions for penny cracks and vesicles (Supplementary Material 3). From these moduli, P- (*Vp*) and S-wave (*Vs*) velocities are estimated for variable porosity, pore shapes and fluid inclusions using water, magma and gas. This model assumes that there is no fluid flow between inclusions (pores or cracks) and is thus applicable to high-frequency measurements. It also assumes inclusions are smaller than the wavelength, randomly distributed, isolated and in small volumes (i.e. low porosity). These assumptions apply well to our set of volcanic rocks measured at ultrasonic frequencies.

## 5 Results

### 5.1 Experimental results

Experimental results are presented in two groups of measurements: The first group consisted of measurements over the volcanic (extrusive and intrusive) and borehole rocks with the aim of studying *Vp/Vs* behaviour with porosity, rock shape, and saturation conditions under effective pressure. The second group focused on the variation of *Vp/Vs* with wave propagation direction in the foliated rocks (Cajamarca Group), that is, wave speed anisotropy.

#### 5.1.1 *Volcanic and borehole rocks*

Figure 4 shows the dry rock *Vp/Vs* ratio as a function of porosity of the NRV volcanic and borehole rocks measured at atmospheric conditions. While *Vp* and *Vs* (Supplementary Material 4) decrease with porosity, *Vp/Vs* increases with increasing porosity in the 6 % to 28 % interval (Figure 4).

Figure 5 shows the *Vp/Vs* ratio versus *Vp* for dry and water-saturated (wet) rocks with increasing depth. Rather than plotting effective pressures, we present the data in terms of the corresponding depth. For that we assume hydrostatic fluid pressures and a rock density of 2545 kg $m^{-3}$ (Supplementary Material 3 shows the corresponding depth to pressure conversion). Volcanics with porosities greater than 6 % and the two borehole rocks are measured dry and water-saturated (Figure 5A), but low-porosity volcanics (<3 %) are only measured dry as saturation was challenging (Figure 5B). To aid the visual interpretation, a linear regression was applied for each rock under both dry and saturated conditions. There is no physical basis for the regression. However, this regres-

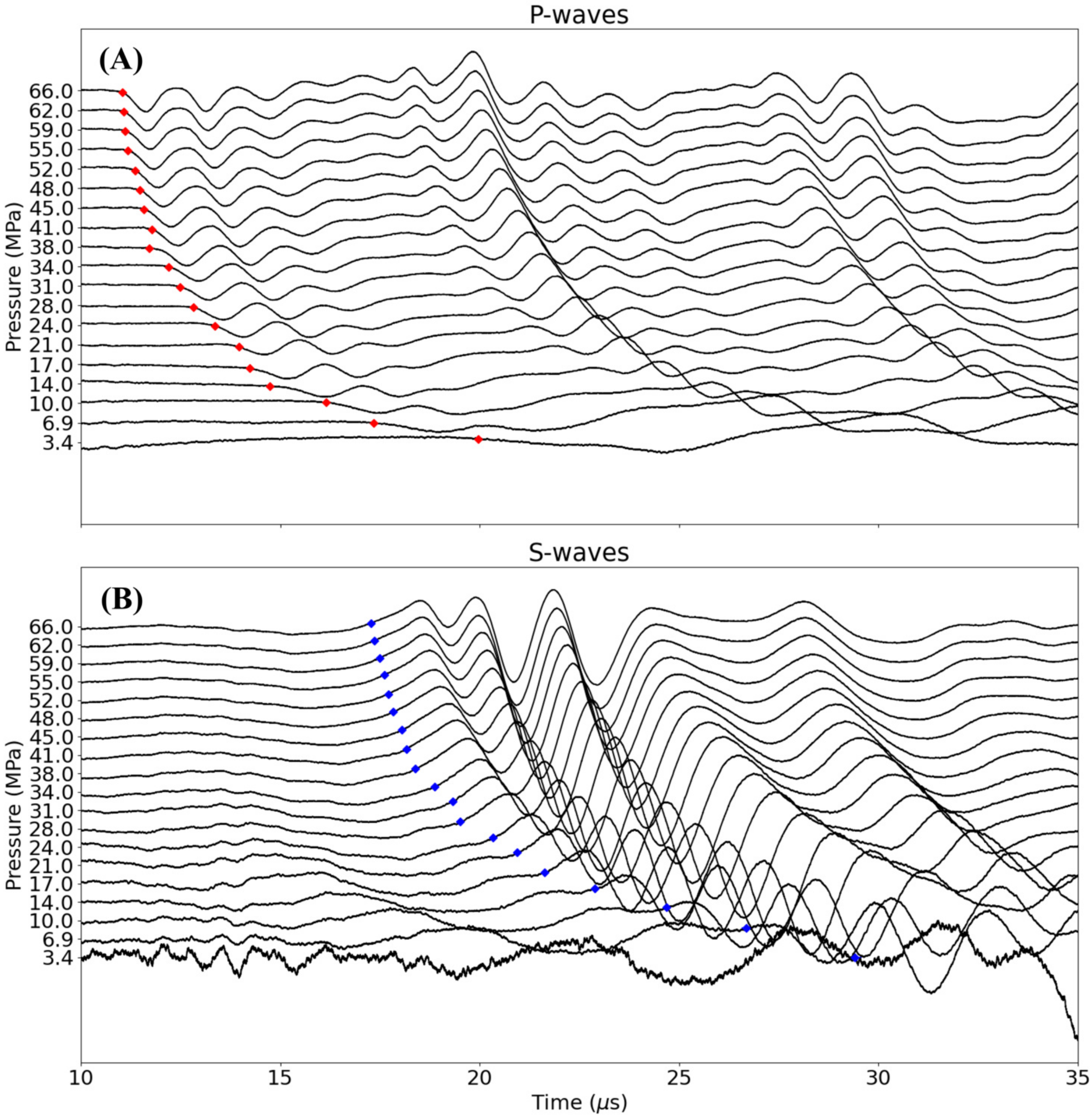


Figure 3: Example of normalized waveforms and time picking for sample SEPR under dry condition: P-wave travel times are shown as red markers [A]; while S-wave travel times in blue [B].

sion is used to estimate the convergence point which would represent the porosity-free *Vp/Vs* and *Vp* of the rock (stars in Figure 5A). Based on these data we observe that 1) *Vp/Vs* ratios (1.45–2.00) and *Vp* (2.50–6.00km s$^{-1}$) span a large domain of values for high-porosity rocks at variable effective pressure and saturation; 2) increasing depth (i.e. effective pressure) significantly increases *Vp* but can either increase (low-porosity rocks) or decrease (high-porosity rocks) *Vp/Vs*, depending on the porosity and fluid type; and 3) the *Vp/Vs* and *Vp* values are influenced by the mineral compositions (porosity-free rocks), but the effect is mostly observed on *Vp*, where shifting of *Vp* along the x-axis is observed).

#### 5.1.2 *Foliated rocks*

Differently from the volcanics, foliated rocks from the Cajamarca Group show a stark relationship between *Vp/Vs*, effective pressure and whether wave propagation is parallel or perpendicular to foliation (Figure 6). Samples where wave propagation was parallel (Meta-1 and Schist-1) or perpendicular (Meta-2 and Schist-2) to foliation have the highest (fast) and lowest (slow) *Vp/Vs*, respectively.

### 5.2 KT model results

We use the Kuster & Toksöz (KT) model [Kuster and Toksöz 1974] to carry out a sensitivity analysis of the relationship between *Vp/Vs* and *Vp* for variable pore shapes [Berryman 1995]. Spheres represent vesicles and penny-shaped cracks represent micro-fractures, and we also present one model of a mixture of both. The analysis also includes porosity reduction in penny-shaped pores to resemble the closure of fractures with effective pressure. Two fluids were modeled: water and

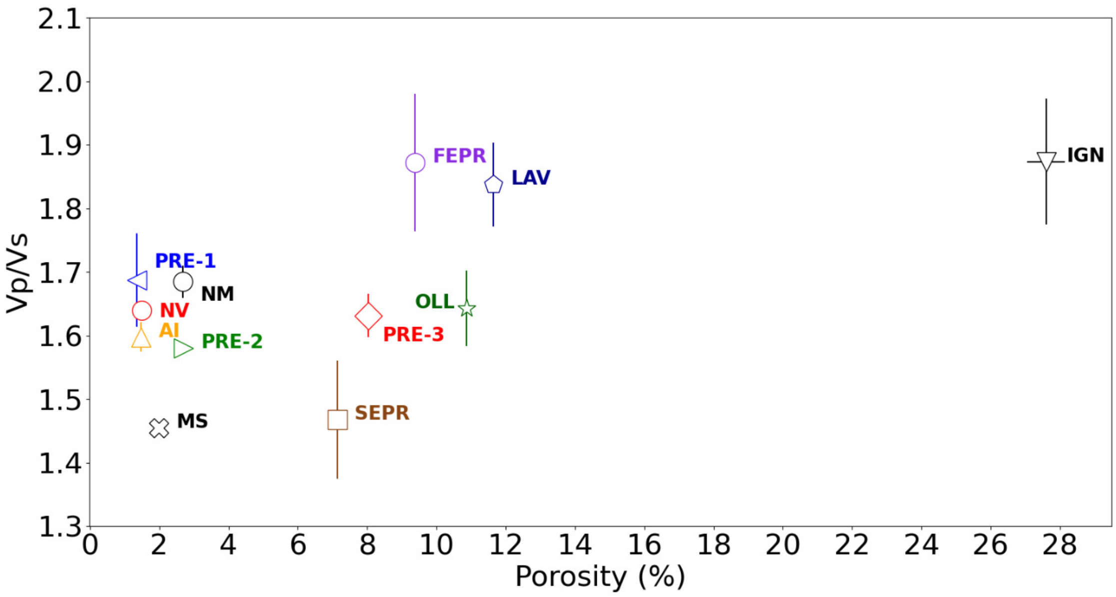


Figure 4: *Vp/Vs* of dry volcanic and borehole rocks at atmospheric pressure as a function of porosity. Bars represent one standard deviation error of the measurements. If bars are not vissible they are smaller in size than the marker. Colours are selected to match rock types as per Figure 2 and symbols are random.

magma. A dry rock is also modeled, which would resemble pores with gas or vapor. The pores of a dry rock would be filled with air. Although the bulk moduli of air, volcanic gas, or water vapor are not identical, in practice, they are many orders of magnitude smaller than those for water or magma. Therefore, for this study we assume that the elastic properties of a dry rock are similar to those with gas or vapor within the pores.

The KT model requires the knowledge of the bulk and shear moduli of the minerals in the rock. Based on the XRD results, we model the dominant four minerals in the NRV rock samples (plagioclase, quartz, K-feldspar, and chlorite). The bulk and shear moduli and density for each mineral are specified in Table 2 [Mavko et al. 2009]. We use a bulk modulus of 2.210 GPa and 0.001 GPa for water and gas at atmospheric temperature and pressure conditions, respectively (NIST Chemistry WebBook*, Lemmon et al. [2005]). For magma, we use the bulk modulus of andesite melt, 16.01 GPa, for a temperature of 1553 Kelvin reported by Schmitt [2015].

Modeled *Vp/Vs* versus *Vp* for spherical inclusions show that when porosity is zero, *Vp/Vs* and *Vp* values converge to that of the mineral assemblage (Figure 7). *Vp/Vs* for magma is greater than for water, which in turn is greater than that of gas. This modelling shows how *Vp/Vs* vs *Vp* can vary significantly due to mineral composition and fluid type.

The KT model of *Vp/Vs* versus *Vp* for penny-shaped inclusions (Figure 8) shows similar trends to those observed for spherical inclusions, but with significantly greater variability

*http://webbook.nist.gov/chemistry

Table 2: Input parameters for the KT modelling. $K$: bulk modulus [GPa]; $G$: Shear modulus [GPa]; $\rho$: density [kg m$^{-3}$].

| Mineral | $K$ | $G$ | $\rho$ |
|---|---|---|---|
| Plagioclase | 75.6 | 25.6 | 2630 |
| K-Feldspar | 37.5 | 15.0 | 2620 |
| Chlorite | 82.6 | 45.1 | 2500 |
| Clinopyroxene | 107.8 | 75.7 | 3200 |
| Quartz | 37.0 | 44.0 | 2700 |

in the *Vp/Vs* and *Vp* space. We used three scenarios of aspect ratios valued from zero up to 0.001, 0.01, and 0.1, respectively. Porosity $X_i$ (Supplementary Material 3) here is represented in terms of the aspect ratio by using a factor $X_i/\alpha$ ranging from zero up to 2.5. Therefore, the porosity modelled is equivalent to 25, 2.5, and 0.25 % for $\alpha$ of 0.1, 0.01, and 0.001, respectively.

In the last model, is where penny-shaped inclusions (of variable porosity $X_i$ and aspect ratio, with $X_i/\alpha$ also ranging from zero up to 2.5) are mixed with 15 % porosity of spherical inclusions. Similar trends as for spherical and penny-shaped pores are observed (Figure 9). However, due to the constant sphere porosity (15 %) in the model, there is no convergence of *Vp/Vs* vs *Vp* even for zero crack porosity. Such a model resembles a rock where cracks close under effective pressure, but not the more spherical pores (vesicles). Stars are the mineral *Vp/Vs*, *Vp* for the four minerals expected when porosity is zero, as shown in Figure 8.

## 6 Discussion

In this section we interpret the controlling physical parameters influencing *Vp/Vs*. The interpretation of *Vp/Vs* is better

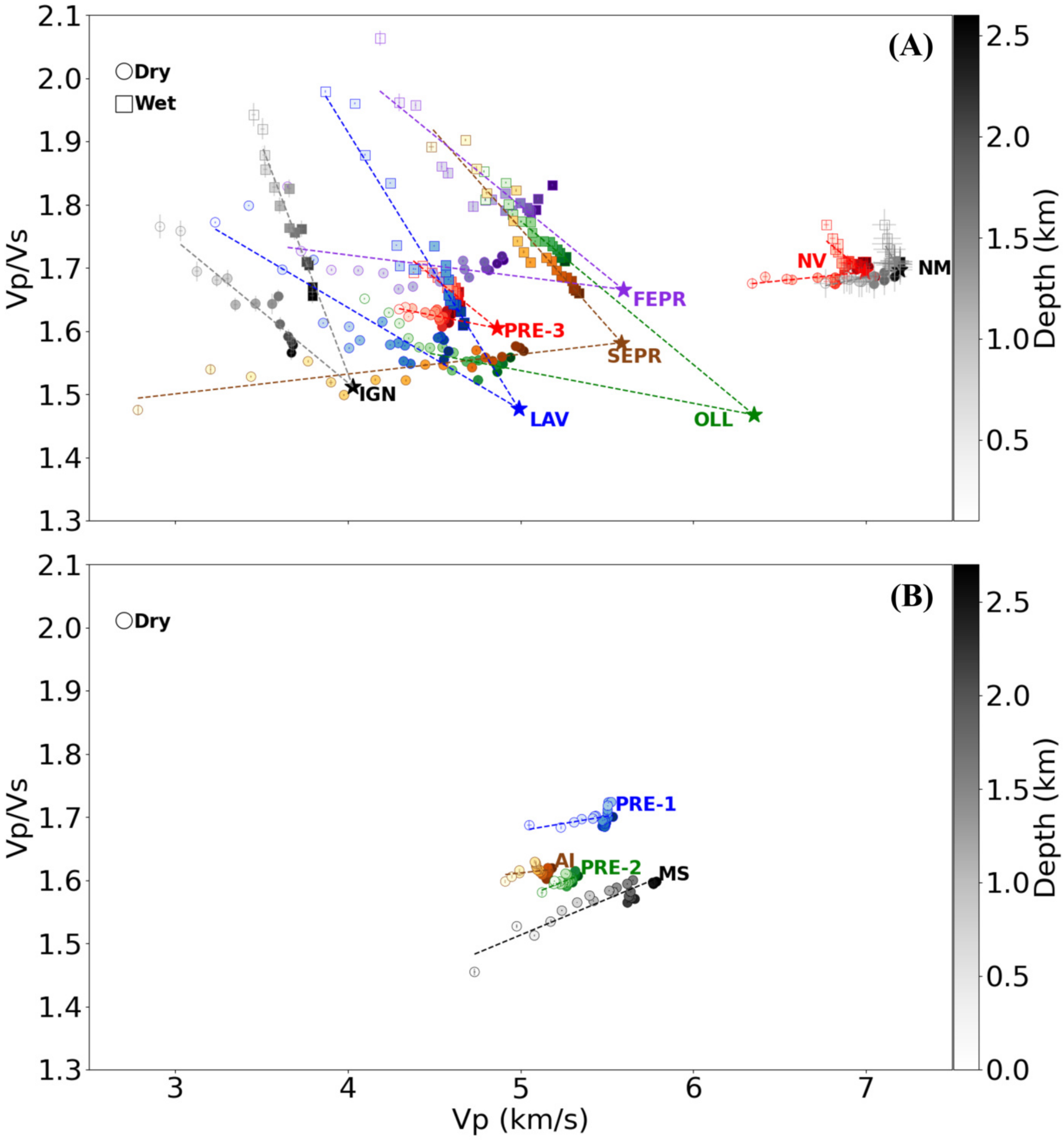


Figure 5: *Vp/Vs* versus *Vp* for [A] high-porosity volcanics (>6 %) and borehole rocks dry (circle) and water-saturated, wet (square) and [B] low-porosity (<3 %) dry rocks. The grayscale indicates the shading associated with depth variations (effective pressure). Dashed lines are linear regressions and stars are convergence values for these regressions resembling a porosity-free rock.

constrained if combined with *Vp*, because P-waves are significantly more sensitive to fluids than S-waves [Ding et al. 2019]. Our discussion focuses on the effect on *Vp/Vs* of porosity, pore shape, fluids, and rock type by integrating laboratory measurements and the KT modeling. Our findings are compiled in Figure 10 and contrasted with typical field *Vp/Vs* values interpreted from seismic inversions at the NRV.

### 6.1 Porosity, pore shapes, and pressure

The broad range of porosities reflects the stratovolcano edifice nature of the NRV (Figure 4). Farquharson et al. [2015] show that for stratovolcanoes (Colima volcano) with effusive and explosive products, a broad range of porosities are expected due to the heterogeneity of the stratigraphic levels. At the NRV, low-porosity rocks are associated with metamorphic and intrusive rocks, as well as the oldest volcanic rock formation PRE. High-porosity rocks correspond to the shallower andesites rocks associated with the latest the NRV eruptive periods. These rocks which contain fractures and vesicles show the highest *Vp/Vs*. High *Vp/Vs* ratios have been reported for ultra-deep carbonates as a result of increasing crack porosity [Markus et al. 2022] and in high-porosity (> 3 %) igneous and metamorphic rocks associated with subduction zones [Peacock et al. 2011; Audet and Schwartz 2013; Audet and Burgmann 2014]. Our results support such observations, where an increase in porosity and fractures could lead to an increase in *Vp/Vs*. On a temporal basis in a volcanic or geothermal setting, an increase in (crack) porosity due to fluid overpressure

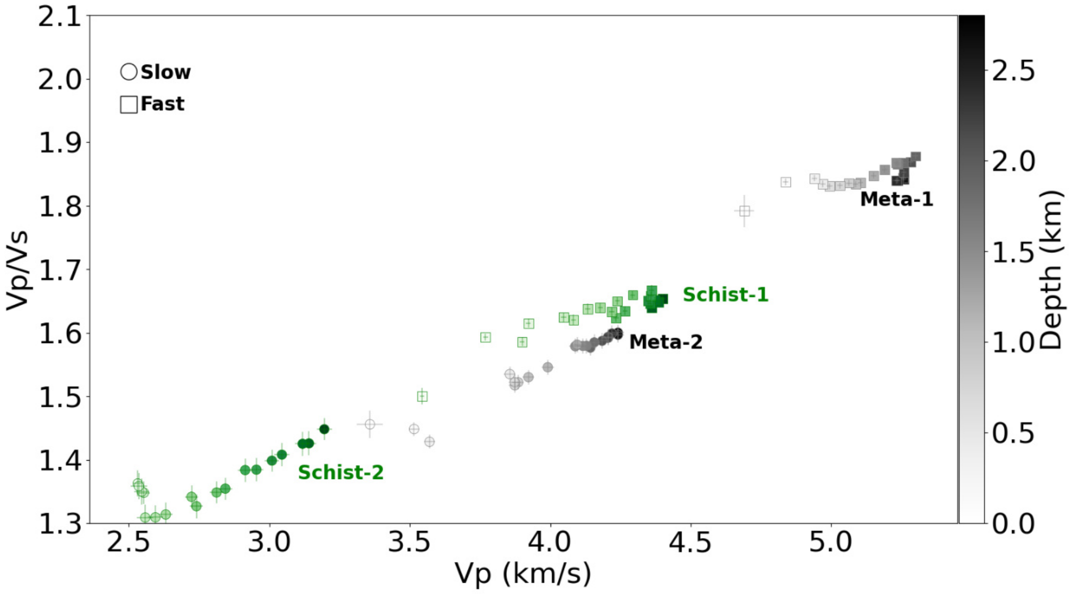


Figure 6: *Vp/Vs* versus *Vp* for dry the NRV foliated rocks (Cajamarca Group). The grayscale indicates the shading associated with depth variations (effective pressure). Marker symbol represents the fast (Meta-1 and Schist-1) and slow (Meta-2 and Schist-2) wave speed propagation directions.

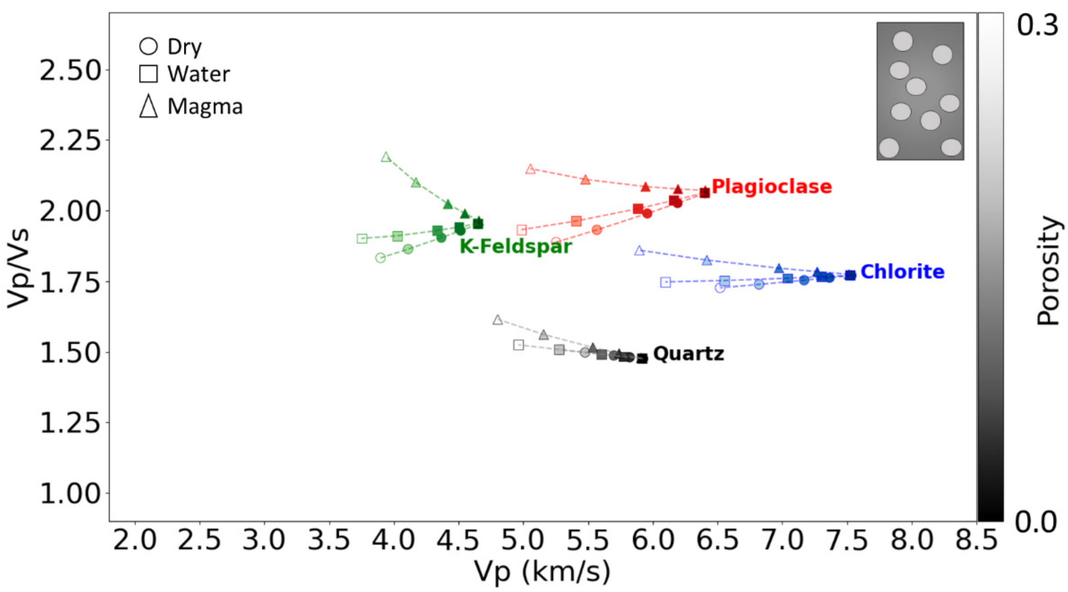


Figure 7: KT modeled *Vp/Vs* vs *Vp* for mixtures of spherical inclusions and four minerals. The colourbar represents porosity variation for each mineral from 0 (darkest) to 0.3 (clearest) as fraction. Three fluids are modeled gas/dry (circles), water (squares) and magma (triangles).

[Pimienta et al. 2018] could increase *Vp/Vs* rather than being due to a change in fluid type.

Volcanic rock porosity can be a mix of vesicles (spherical pores) and fractures (ellipsoidal or penny-shaped cracks) [Wang 2001; Hook 2003; Rejeki et al. 2005; Adam et al. 2013; Saxena et al. 2018; Duran et al. 2019b; Mordensky et al. 2019]. For rocks comprised mostly of vesicles, wave speeds are less sensitive to increasing effective pressures (i.e. depth), while the presence of cracks results in significant wave speed variation with pressure [Walsh 1965; Wang et al. 2005; Duran et al. 2019b; Adam et al. 2020]. In other words, cracks (low aspect ratio pores) are highly compressible while vesicles are

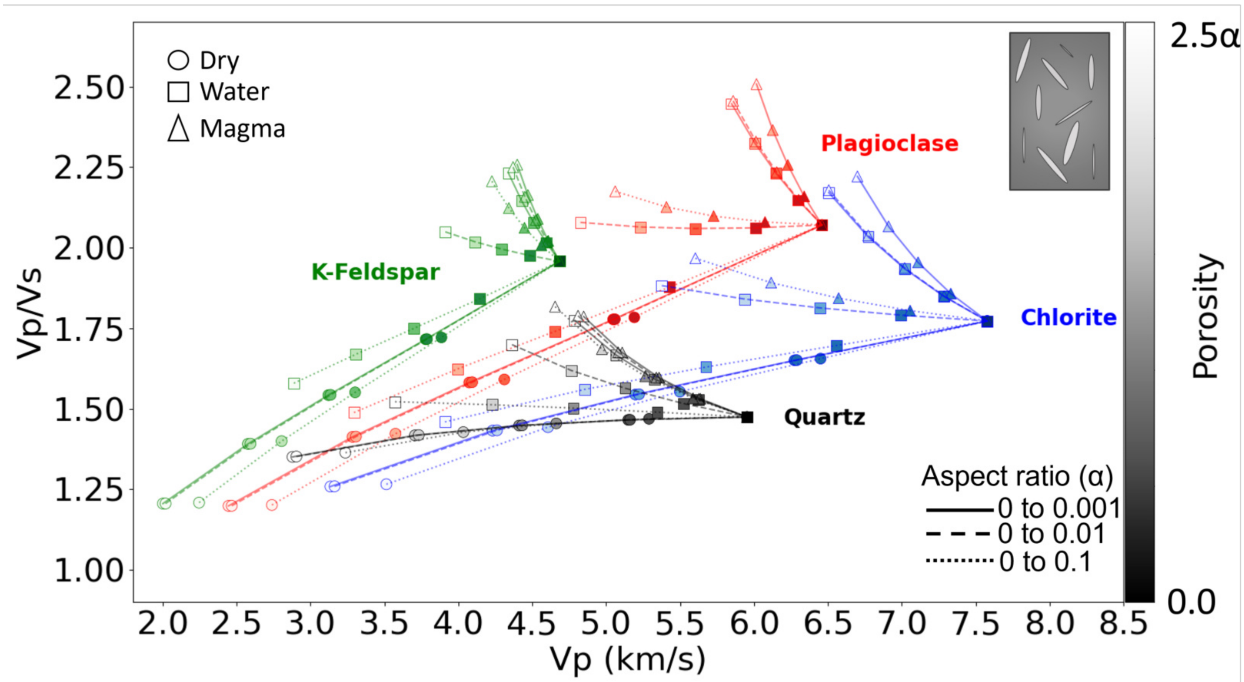


Figure 8: KT's model of *Vp/Vs* vs *Vp* for penny-shaped inclusions. The colourbar represents the colour tone for the markers indicating the porosity $X_i$ variation for each mineral from 0.0 (darkest) to the highest value of 2.5α (clearest). $X_i$ is indicated as a function of the aspect ratio α with the factor 2.5 as the highest value of $X_i/\alpha$, starting from zero. Three fluids are modeled gas/dry (circles), water (squares) and magma (triangles).

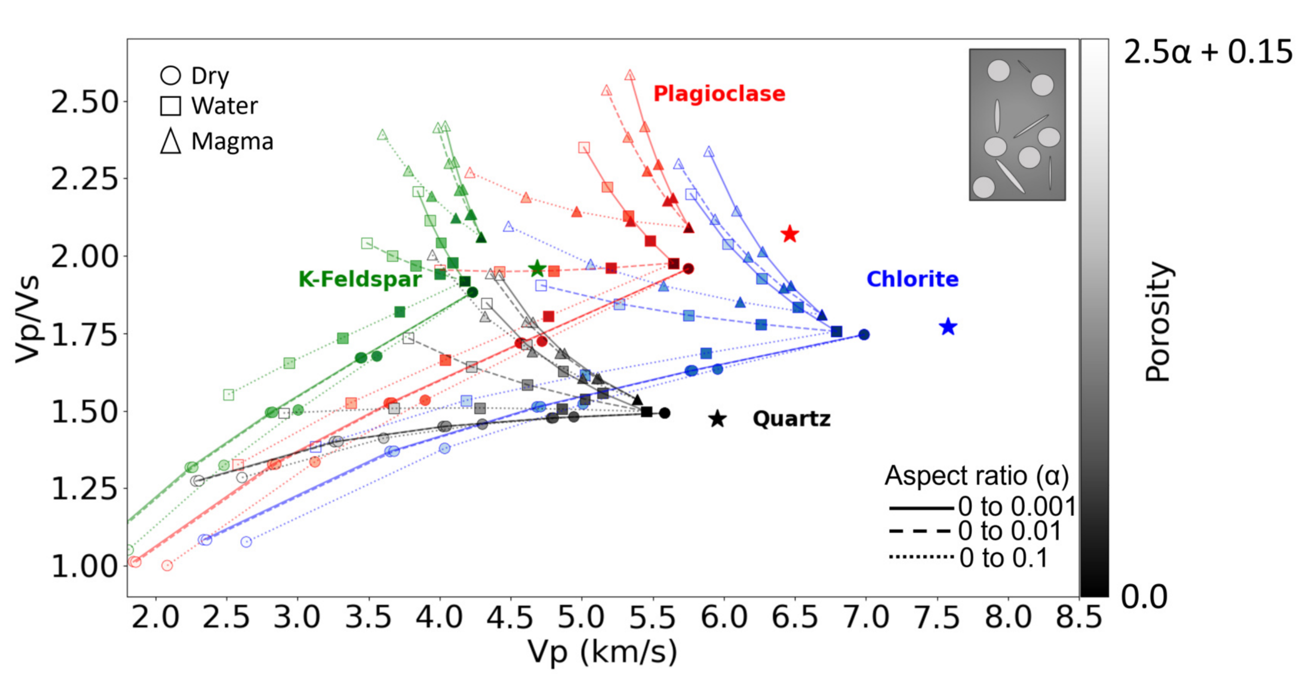


Figure 9: KT model for a mix of penny-shaped inclusions plus a constant of 15 % porosity due to sphere inclusions: *Vp/Vs* versus *Vp*. The colourbar represents the colour tone for the markers indicating the porosity variation for each mineral from 0.0 (darkest) to the highest value of 2.5α + 0.15 (clearest). The porosity associated with penny-shaped inclusions $X_i$ is indicated as a function of the aspect ratio α with the factor 2.5 as the highest value of $X_i/\alpha$ starting from zero. Three fluids are modeled gas (circles), water (squares) and magma (triangles).

poorly compressible. Therefore, varying the pore shape and volumes with the KT model resembles the experimental observations of pore closure with effective pressure (i.e. depth).

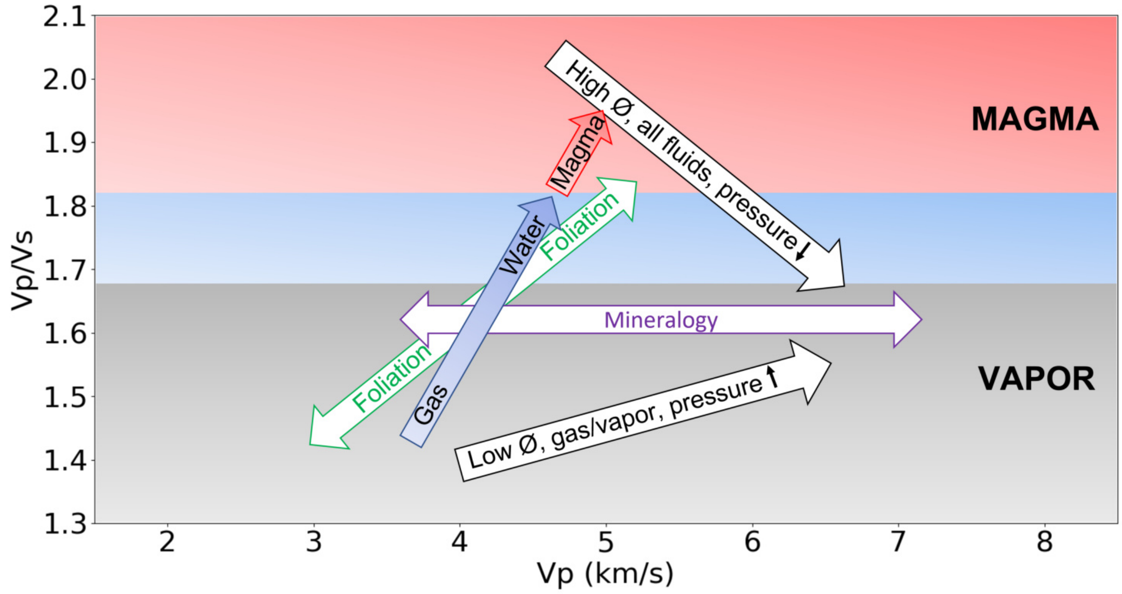


Figure 10: Comparison of *Vp/Vs* vs *Vp* from experimental, modeling and field interpretations. Background colours of *Vp/Vs* are field interpretations [Vargas et al. 2017; Londono and Kumagai 2018] for magma (red) and gas/vapor (grey). Blue and red arrows with gradients are dry-to-water water-to-magma effect on *Vp/Vs-Vp* from our KT analysis. Green outlined arrow is experimental foliated-induced anisotropy effect on *Vp/Vs-Vp*. Black outlined arrows compile the general trend porosity, effective pressure (depth) and fluids induce on *Vp/Vs-Vp* from experiments and KT modeling. This is presented for two cases: dry/gas/vapor low-porosity rocks and fluid-saturated high-porosity rocks. Purple arrow is the average behaviour of *Vp/Vs-Vp* with mineralogy.

Our measurements supported with the KT modeling show that (Figure 10):

- For a range of porosities, *Vp/Vs* varies significantly in the presence of cracks (Figure 7) when compared to a rock with spherical inclusions (Figure 8). Therefore, highly fractured rocks have higher *Vp/Vs* to *Vp* sensitivity to effective pressure (i.e. depth) than rocks dominated by vesicles.

- In the presence of a mixture of cracks and spheres (Figure 9), when cracks close at high pressures, the vesicular pores remain open, resulting in wave speeds that do not reach those of the minerals (i.e. porosity-free rocks).

- For dry/gas-saturated rocks, we see two trends. If porosity is below 6 %, then *Vp/Vs* increases with effective pressure (depth). For high-porosity rocks (> 6 %), *Vp/Vs* decreases with increasing effective pressure for all fluids.

### 6.2 Fluids

Because most liquids (e.g. water, magma) are poorly-compressible or incompressible, increasing fluid saturation reduces the compressibility of the pore space, resulting in an overall increase of the rock's bulk modulus, and thus P-wave velocity [Saxena et al. 2018]. The change in bulk modulus due to saturation is much higher than that of the density. The rock shear modulus is insensitive to fluids; however, the density of the rock changes with the type of saturating fluid. Therefore, fluids influence S-wave speeds, when the density of a rock increases, the S-wave speed decreases. The *Vp/Vs* ratio eliminates the contributions from density, and therefore only senses the bulk to shear moduli ratio, and is therefore commonly linked to changes in fluids types. Our KT modeling combined with experimental data shows (Figure 10):

- An increase in fluid bulk moduli (i.e. change in fluid type) increases *Vp/Vs* ( Figures 5, 7, 8, and 9). The higher the bulk modulus of the fluid (Table 2), the greater the change in *Vp/Vs* (e.g. *Vp/Vs*-magma > *Vp/Vs*-water > *Vp/Vs*-gas).

- *Vp/Vs* is most sensitive to fluid type for rocks with cracks compared to those with vesicles (Figures 8 and 9).

Samples FEPR, OLL, SEPR, LAV, and IGN show high pressure dependence of *Vp/Vs* and *Vp*. This is interpreted as being due to the presence of cracks (Figure 5) and results in greater *Vp/Vs* to water vs air. In comparison, sample PRE-3 shows little *Vp/Vs* response to pressure, interpreted as a rock dominated by vesicles, resulting in poor *Vp/Vs* sensitivity to fluids.

### 6.3 Rock type—mineralogy

The rock elastic response is also influenced by its mineral composition [Castagna et al. 1985; Christensen 1996; Pola et al. 2012; Siratovich et al. 2014; Wilkens et al. 2018; Duran et al. 2019b]. For a porosity-free rock, only the mineral content of the rock determines the *Vp/Vs*. Because the mineralogy of volcanics is highly variable we model wavespeeds and *Vp/Vs* for a range of key minerals.

As expected, as porosity decreases, *Vp/Vs* vs *Vp* trends towards the values representative of the mineral (Figure 7).

However, when there is open porosity remaining (e.g. vesicles) and all the crack porosity is closed, the dry and water-saturated velocity trends do not converge to that of the mineral (Figure 9). Modeled *Vp/Vs* for porosity-free rocks (convergent points in Figure 7) shows that the mineralogy alone influences the *Vp/Vs* ratio. The effect of different minerals has a stronger effect on *Vp* than on *Vp/Vs*. This is observed by the shifting of porosity-free data along the *Vp*-axis (Figure 10 and Figure 7). We only modeled common volcanic minerals, but it is recommended that all minerals, including any alteration minerals, are quantified via XRD analysis and used to model *Vp* and *Vs* to understand the influence of mineralogy on *Vp/Vs*.

From our experimental data, we only reach the porosity-free *Vp/Vs* (i.e. pressure dependence convergence) for the borehole samples (NM, NV) (Figure 5 compared to Figure 7). These rocks have high fluid and pressure sensitivity pointing at the presence of fractures which mostly close at 40 MPa (~1.6 km depth). Importantly, the presence and closure of fractures is observed for both the matrix of the borehole sample (NM) and for the same rock with a quartz alteration vein (NV). Our other measured rocks do not show this convergence meaning that porosity remains open even at effective pressures of ~60 MPa. In this study we did not characterize the effect of hydrothermal alteration on *Vp/Vs* as systematic sampling was not possible due to the lack of outcrop exposures for such tasks. However, mineral alteration plays a significant role in changing the porosity of rocks by precipitation and/or dissolution of minerals [Pola et al. 2014; Mayer et al. 2016; Kanakiya et al. 2017; Mordensky et al. 2018; Kanakiya et al. 2021] which in turn will increase or decrease the *Vp* and *Vs* in those rocks.

### 6.4 Foliation-induced anisotropy

Visual and microphotograph foliation (Supplementary Material 1) is observed for rocks from the Cajamarca Group, resulting in the directional dependence of wave speeds (i.e. wave speed anisotropy). For our dry rocks measured under effective pressure, *Vp/Vs* is higher for waves with particle motion (i.e. polarization) parallel to the foliation plane (samples Schist-1 and Meta-1), but lower when this motion is perpendicular to foliation (samples Schist-2 and Meta-2) (Figure 6, see Supplementary Material 4). Our results are similar to those of Fliedner and French [2021] and Miller et al. [2021] on metasedimentary rocks under dry conditions. In our study, *Vp/Vs* can span a range of 1.3–1.9 only as a result of elastic wave anisotropy. Anisotropy can also be due to aligned fractures which due to volcanic processes can open/close or change directions over time [Savage et al. 2010]. Therefore, it is clear that wave anisotropy has significant impacts on *Vp/Vs* values and could be misinterpreted as fluids or pressure variations (Figure 10) [Christensen 2004; Song and Kim 2012]. Such observations are critical for the NRV geothermal system as the targeted resources reside in foliated metamorphic rocks [Monsalve et al. 1998; Vélez et al. 2018].

### 6.5 Field implications

Boitnott [1995] and Boitnott and Kirkpatrick [1997] found that at The Geysers (USA), elastic wave in-situ laboratory data are more representative of the matrix properties of the rocks. They argue that the influence of field-scale compliant features (e.g. joints and faults) on wave speeds decreases with depth. Likewise, Moos and Zoback [1983] found that field seismic wave speeds of crystalline rocks with low macroscopic fractures densities are similar to experimentally measured water-saturated rocks under effective pressure. Therefore, our experimental observations on the effects of fluids, micro-cracks and mineralogy at in-situ pressure conditions could be used to aid the field seismic interpretation of the deeper crust at the NRV. The effect of each of these parameters is summarized in Figure 10 and compared to the field *Vp/Vs* values from Londono and Kumagai [2018].

The significant decrease of *Vp/Vs* with depth for most of our samples (Figure 5) is supported by observations from Romero-Jr et al. [1995] and Boitnott and Kirkpatrick [1997] at The Geysers (USA), Markus et al. [2022] for ultra-deep carbonates and Peacock et al. [2011] for igneous and metamorphic rocks associated with subduction zones. However, for low-porosity rocks (AI, PRE-1, PRE-2 and PRE-3, NM, NV) the *Vp/Vs* is only slightly sensitive to effective pressure.

*Vp/Vs* is commonly used as an indicator of vapor, water, or magma within the rocks [Moos and Zoback 1983; Chatterjee et al. 1985; Boitnott and Kirkpatrick 1997; Nakajima et al. 2001b; Conder and Wiens 2006; Gritto et al. 2013; Muksin et al. 2013; Gritto and Jarpe 2014; Gritto et al. 2014; Lin and Wu 2018]. Dry experimental conditions are equivalent to gas (e.g. vapour) as long as the fluid pressures are not too high [Mavko et al. 2009]. The common relation that *Vp/Vs* magma > *Vp/Vs* water > *Vp/Vs* dry has been modeled and widely used to interpret fluids beneath volcanoes [Nakajima et al. 2001a; b; Koulakov et al. 2013; Kasatkina et al. 2014; Vargas et al. 2017]. In seismic inversions, low *Vp/Vs* (ranging commonly between 1.3 and 1.7) is interpreted as vapor/gas dominated reservoirs, while high *Vp/Vs* (ranging commonly from 1.8 to 2.1) is associated with fluids [Romero-Jr et al. 1995; Gritto et al. 2013; Londono and Kumagai 2018]. In the case of the NRV, high *Vp/Vs* anomalies from seismic tomography sections are interpreted as magma chamber locations, magma injection and degassing processes [Londono 2010; Kasatkina et al. 2014; Vargas et al. 2017; Londono and Kumagai 2018]. For instance, a spatial *Vp/Vs* anomaly (ranging from 1.8 to 2.2) at depths of 2–5 km below the NRV summit is interpreted as a shallow magma reservoir [Vargas et al. 2017]. Likewise, Londono and Kumagai [2018] estimates *Vp/Vs* values higher than 1.9 at depths of 2 to 3 km beneath the volcano active crater, once more interpreted as magma. Vargas et al. [2017] also investigate temporal changes in *Vp/Vs* at the NRV. A decrease of *Vp/Vs* by ~0.5 from 2010 to 2014 is interpreted as being due to gas eruptions; followed by an increase of *Vp/Vs* later in time (2015 to 2016) interpreted as new magma injection beneath the NRV [Vargas et al. 2017]. In addition to fluid, our experimental data on the NRV rocks show that such increases and decreases in *Vp/Vs* ratios can also be explained as changes in effective pressure, open pore shapes, and mineralogy (Figure 10).

Our KT model shows that mineralogy controls the porosity-free *Vp/Vs*. For instance, quartz has a lower *Vp/Vs* than plagioclase (e.g. Figure 7). Field examples also suggest that lithology controls *Vp/Vs* variations: Audet and Burgmann [2014] show that silica enrichment decreases *Vp/Vs*; Nakajima et al. [2001b] found that *Vp/Vs* increases from the upper crust to the uppermost mantle due to possibly of changes in lithology; and Boitnott and Kirkpatrick [1997] reported an increase in *Vp/Vs* that correlates with illite content due to chemo-mechanical weakening. By applying linear regressions to the experimental data (*Vp/Vs* vs *Vp*) with pressure, we observe that the NRV rocks have significantly varying mineralogy as the lines converge to a range of *Vp/Vs* vs *Vp* (stars in Figure 5). Nonetheless, we can see that the effect of mineralogy mostly shifts the data along the *Vp* axis as it is sketched in Figure 10. The data presented here represent the rock matrix and the micro-fractures within. Macro-fractures could lower the wave speeds even more significantly [Moos and Zoback 1983; Nara et al. 2011] from the compliance of the fractures or scattering from them.

Foliated rocks show elastic wave anisotropic behavior at the field scale [Christensen 1965; Johnson and Wenk 1974; Ji and Salisburyb 1993; Christensen 2004; Song and Kim 2012; Rabbel et al. 2017; Fliedner and French 2021; Kästner et al. 2021; Miller et al. 2021]. Commonly, studies focus on estimating P- and S-wave directional behaviour and have seldom made the link to *Vp/Vs* ratio interpretations. That is because defining which propagation and particle motion directions are used to estimate *Vp/Vs* is less understood. Wang et al. [2012] has shown that anisotropic *Vp/Vs* can be lower than 1.3 in fractured rocks. Here we present *Vp/Vs* ratios based in the polarization of the waves, parallel and perpendicular to layering. We show that *Vp/Vs* is high when wave polarization is parallel to the foliation plane. The same would apply if anisotropy is due to aligned fractures, *Vp/Vs* for polarizations parallel to the fracture plane would be highest [Wang et al. 2012]. The implications to the field are clear: high *Vp/Vs*, typically associated with fluid saturation (water or magma), could actually be due to rocks with foliation or open aligned fractures. Likewise, we show that low *Vp/Vs* could be associated witho wave polarization perpendicular to the foliation plane rather than due to vapor/gas (Figure 10).

We only investigated rock property relationships with *Vp/Vs* under effective pressure. The influence of temperature on the elastic rock behavior has not been taken into consideration here. However, it has been demonstrated that temperature influences the elastic rock properties [Spencer-Jr and Nur 1976; Timur 1977; Jones et al. 1980; Matsumoto et al. 1986; Nakajima et al. 2001b; Jaya et al. 2010; Saxena et al. 2018; Simpson et al. 2019]. Therefore, research is needed to understand how porosity, mineralogy, and saturating fluids influence *Vp/Vs* with temperature.

## 7 Conclusions

Our experimental data and numerical models of *Vp* and *Vs* for the NRV rock formations show that *Vp/Vs* is influenced by pore shape, effective pressures, fluids, and rock lithology. We highlight that changes in *Vp/Vs* ratio for a range of volcanic and metamorphic lithologies goes beyond a fluid-type effect. Porosity and the presence of cracks versus vesicular pores controls whether *Vp/Vs* increases or decreases with fluids and pressure. Mineralogy changes influence *Vp* much more significantly than *Vp/Vs*. Our experimental *Vp/Vs* values for the different samples collected from the NRV are consistent with the ranges reported by the seismic tomographies in the area. In this study we provide alternative reasons on why *Vp/Vs* changes beyond changes in fluids types, such as fractures shape and volume, anisotropy, and mineralogy.

## Author Contributions

JPAB conducted fieldwork, data collection, and wrote the manuscript. LA contributed to data collection, writing and editing.

## Acknowledgements

We thank the SGC for the support on the fieldwork. The Ministry of Foreign Affairs and Trade (MFAT) New Zealand development scholarship is acknowledged for the funding offered to JPAB for his doctorate studies in New Zealand. We immensely appreciate the guidance for the field trip offered by the Colombian Geological Survey, specially to María Luisa Monsalve and Lilly Martínez, and by the Universidad de Caldas' students Peter Macías, Luis Alvaro Botero and Gabriel Granja. We also thank Julian López from CHEC-EPM for providing the samples from the geothermal well Nereidas-1. We acknowledge the technical support from Phil White from PandaGeoscience, Michael Rowe and Andrés Arcila from The University of Auckland with the thin sections and XRD analysis. We greatly thank Dr. Cédric Bailly and Dr. Oliver Lamb for their feedback on the manuscript, as well as Associate Editor Dr. Alexandra R. L. Kushnir for her comments.

## Data Availability

Data for the Figures 4, 5, and 6 is available to be downloaded from https://doi.org/10.5281/zenodo.7519960. Supplementary Material is available alongside the online version of this article.

## Copyright notice



## References

Adam, L., M. Frehner, K. Sauer, V. Toy, and S. Guerin-Marthe (2020). "Seismic anisotropy and its impact on imaging the Alpine Fault: an experimental and modeling perspective". *Journal of Geophysical Research: Solid Earth* 125, e2019JB019029. DOI: https://doi.org/10.1029/2019JB019029.

Adam, L., K. Wijk, T. Otheimand, and M. Batzle (2013). "Changes in elastic wave velocity and rock microstructure due to basalt-CO2-water reactions". *Journal of Geophysical Research: Solid Earth* 118, pages 4039–4047. DOI: 10.1002/jgrb.50302.

Amalokwu, K., A. I. Best, and M. Chapman (2016). "Effects of aligned fractures on the response of velocity and attenuation ratios to water saturation variation: a laboratory study using synthetic sandstones". *Geophysical Prospecting* 64, pages 942–957. DOI: 10.1111/1365-2478.12378.

Audet, P. and R. Burgmann (2014). "Possible control of subduction zone slow-earthquake periodicity by silica enrichment". *Nature* 510(7505), pages 389–392. DOI: 10.1038/nature13391.

Audet, P. and S. Y. Schwartz (2013). "Hydrologic control of forearc strength and seismicity in the Costa Rican subduction zone". *Nature Geoscience* 6(10), pages 852–855. DOI: 10.1038/ngeo1927.

Batzle, M. and Z. Wang (1992). "Seismic properties of pore fluids". *Geophysics* 57(11), pages 1396–1408. DOI: 10.1190/1.1443207.

Baxter, P. J., C. Bonadonna, R. Dupree, V. L. Hards, S. C. Kohn, M. D. Murphy, A. Nichols, R. A. Nicholson, G. Norton, A. Searl, R. S. J. Sparks, and B. P. Vickers (1999). "Cristobalite in volcanic ash of the Soufriere Hills Volcano, Montserrat, British West Indies". *Science* 283(5405), pages 1142–1145. DOI: 10.1126/science.283.5405.1142.

Berryman, J. G. (1995). *Rock Physics and Phase Relations, chap. Mixture Theories for Rock Properties*. American Geophysical Union. DOI: https://doi.org/10.1029/RF003p0205.

Boitnott, G. N. (1995). "Laboratory measurements on reservoir rocks from The Geysers geothermal field". *Proceedings 20th Workshop on Geothermal Reservoir Engineering, Stanford University, California*, pages 107–114.

Boitnott, G. N. and A. Kirkpatrick (1997). "Interpretation of field seismic tomography at The Geysers geothermal field, California". *Proceedings 22th Workshop on Geothermal Reservoir Engineering, Stanford University, California*, pages 391–398.

Brantut, N. and E. C. David (2018). "Influence of fluids on Vp/Vs ratio: Increase or decrease?" *Geophysical Journal International* 216(3), pages 2037–2043. DOI: 10.1093/gji/ggy518.

Castagna, J. P. and M. M. Backus (1993). *Offset-dependent reflectivity-Theory and practice of AVO analysis*. Society of Exploration Geophysicists. DOI: https://doi.org/10.1190/1.9781560802624.fm.

Castagna, J. P., M. L. Batzle, and R. L. Eastwood (1985). "Relationships between compressional-wave and shear-wave velocities in clastic silicate rocks". *Geophysics* 50, pages 571–581. DOI: 10.1190/1.1441933.

Ceballos-Hernandez, J. A., L. M. Martinez-Tabares, L. G. Valencia-Ramirez, B. A. Pulgarin-Alzate, A. M. Correa-Tamayo, and B. L. Narvaez-Marulanda (2020). "Geological evolution of the Nevado del Ruiz Volcanic Complex". *Publicaciones Geológicas Especiales* 68, pages 267–296. DOI: 10.32685/pub.esp.38.2019.07.

Chatterjee, S. N., A. M. Pitt, and H. M. Iyer (1985). "Vp/Vs ratios in The Yellowstone National Park Region, Wyoming". *Journal of Volcanology and Geothermal Research* 26(3–4), pages 213–230. DOI: 10.1016/0377-0273(85)90057-5.

Chiarabba, C. and M. Moretti (2006). "An insight into the unrest phenomena at the Campi Flegrei caldera from Vp and Vp/Vs tomography". *Terra Nova* 18(6), pages 373–379. DOI: 10.1111/j.1365-3121.2006.00701.x.

Christensen, N. I. (1965). "Compressional wave velocities in metamorphic rocks at pressures to 10 kilobars". *Journal of Geophysical Research* 70(24), pages 6147–6164. DOI: 10.1029/JZ070i024p06147.

– (1996). "Poisson's ratio and crustal seismology". *Journal of Geophysical Research* 101(B2), pages 3139–3156. DOI: 10.1029/95JB03446.

– (2004). "Serpentinites, Peridotites, and Seismology". *International Geology Review* 46(9), pages 795–816. DOI: 10.2747/0020-6814.46.9.795.

Conder, J. A. and D. A. Wiens (2006). "Seismic structure beneath the Tonga arc and Lau back-arc basin determined from joint Vp, Vp/Vs tomography". *Geochemistry, Geophysics, Geosystems* 7(3). DOI: 10.1029/2005GC001113.

De Hoog, J. C. M., M. J. van Bergen M J, and M. H. G. Jacobs (2019). "Vapour-phase crystallisation of silica from SiF4-bearing volcanic gases". *Annals of Geophysics* 48(4–5), pages 775–785. DOI: 10.4401/ag-3233.

Delliansyah, R., R. Sule, and A. D. Nugraha (2015). "Steam and Brine Zones Prediction Inside an Operated Geothermal Reservoir Based on Seismic Velocities Produced by Double Difference Tomography". *Proceedings World Geothermal Congress*, pages 19–25.

Ding, P., D. Wang, G. Di, and X. Li (2019). "Investigation of the effects of fracture orientation and saturation on the Vp/Vs ratio and their Implications". *Rock Mechanics and Rock Engineering* 52, pages 3293–3304. DOI: 10.1007/s00603-019-01770-3.

Duran, E. L., L. Adam, and I. Wallis (2019a). "A robust methodology for time picking and error analysis of ultrasonic waveforms and rock densities in the laboratory". *Geophysics* 84(2), pages 1–13. DOI: 10.1190/geo2018-0331.1.

Duran, E. L., L. Adam, I. C. Wallis, and A. Barnhoorn (2019b). "Mineral alteration and fracture influence on the elastic properties of volcaniclastic rocks". *Journal of Geophysical Research: Solid Earth* 124(5), pages 4576–4600. DOI: 10.1029/2018JB016617.

Farquharson, J., M. J. Heap, N. R. Varley, P. Baud, and T. Reuschlé (2015). "Permeability and porosity relationships of edifice-forming andesites: A combined field and laboratory study". *Journal of Volcanology and Geothermal Research* 297, pages 52–68. DOI: 10.1016/j.jvolgeores.2015.03.016.

Fliedner, C. and M. E. French (2021). "Pore and mineral fabrics control the elastic wave velocities of metapelite with implications for subduction zone tomography". *Journal of Geophysical Research: Solid Earth* 126(10), pages 1–24. DOI: 10.1029/2021JB022361.

Forero, J., C. A. Zuluaga, and J. Mojica (2011). "Alteration related to hydrothermal activity of the Nevado del Ruiz volcano (NRV), Colombia". *Boletin de Geologia* 33(1), pages 59–67.

Getahun, A., M. H. Reed, and R. Symonds (1996). "Mount St. Augustine volcano fumarole wall rock alteration: mineralogy, zoning, composition and numerical models of its formation process". *Journal of Volcanology and Geothermal Research* 71(2-4), pages 73–107. DOI: 10.1016/0377-0273(95)00071-2.

González-García, J., J. Hauser, D. Annetts, J. Franco, E. Vallejo, and K. Regenauer-Lieb (2015). "Nevado Del Ruiz Volcano (Colombia): A 3D model combining geological and geophysical information". *Proceedings World Geothermal Congress*, pages 1–11.

Gritto, R. and S. P. Jarpe (2014). "Temporal variations of Vp/Vs-ratio at The Geysers geothermal field, USA". *Geothermics* 52, pages 112–119. DOI: 10.1016/j.geothermics.2014.01.012.

Gritto, R., A. E. Romero, and T. M. Daley (2014). "Results of a VSP experiment at the Resurgent Dome, Long Valley caldera, California". *Geophysical Research Letters* 31(6), page L06603. DOI: 10.1029/2004GL019451.

Gritto, R., S. Yoo, and S. P. Jarpe (2013). "Three-dimensional seismic tomography at The Geysers geothermal field, CA, USA". *Proceedings 38th Workshop on Geothermal Reservoir Engineering Stanford University, Stanford, California*.

Hook, J. R. (2003). "An introduction to porosity". *Petrophysics* 44(3), pages 205–212.

Jaya, M. S., S. A. Shapiro, L. H. Kristinsdóttir, D. Bruhn, H. Milsch, and E. Spangenbergc (2010). "Temperature dependence of seismic properties in geothermal rocks at reservoir conditions". *Geothermics* 39(1), pages 115–123. DOI: 10.1016/j.geothermics.2009.12.002.

Ji, S. and M. H. Salisburyb (1993). "Shear-wave velocities, anisotropy and splitting in high-grade mylonites". *Tectonophysics* 221(3–4), pages 453–473. DOI: 10.1016/0040-1951(93)90173-H.

Johnson, L. R. and H. R. Wenk (1974). "Anisotropy of physical properties in metamorphic rocks". *Tectonophysics* 23(1–2), pages 79–98. DOI: 10.1016/0040-1951(74)90112-7.

Jones, T., W. Murry, and A. Nur (1980). "Effects of temperature and saturation on the velocity and attenuation of seismic waves in rocks: Applications to geothermal reservoir evaluation". *Proceedings Stanford Geothermal Workshop*, pages 328–337.

Kanakiya, S., L. Adam, L. Esteban, M. C. Rowe, and P. Shane (2017). "Dissolution and secondary mineral precipitation in basalts due to reactions with carbonic acid". *Journal of Geophysical Research: Solid Earth* 122(6), pages 4312–4327. DOI: 10.1002/2017JB014019.

Kanakiya, S., L. Adam, M. C. Rowe, J. M. Lindsay, and L. Esteban (2021). "The role of tuffs in sealing volcanic conduits". *Geophysical Research Letters* 48(20), e2021GL095175. DOI: 10.1029/2021GL095175.

Kasatkina, E., I. Koulakov, M. West, and P. Izbekov (2014). "Seismic structure changes beneath Redoubt Volcano during the 2009 eruption inferred from local earthquake tomography". *Journal of Geophysical Research: Solid Earth* 119(6), pages 4938–4954. DOI: 10.1002/2013JB010935.

Kästner, F., S. Pierdominici, A. Zappone, L. F. G. Morales, A. M. Schleicher, F. D. H. Wilke, and C. Berndt (2021). "Cross-scale seismic anisotropy analysis in metamorphic rocks from the COSC-1 borehole in the Scandinavian Caledonides". *Journal of Geophysical Research: Solid Earth* 126(5), pages 1–25. DOI: 10.1029/2020JB021154.

Koulakov, I., M. West, and P. Izbekov (2013). "Fluid ascent during the 2004–2005 unrest at Mt. Spurr inferred from seismic tomography". *Geophysical Research Letters* 40(17), pages 4579–4582. DOI: 10.1002/grl.50674.

Koulakov, I., T. Yudistira, B.-G. Luehr, and Wandono (2009). "P, S velocity and VP/VS ratio beneath the Toba caldera complex (Northern Sumatra) from local earthquake tomography". *Geophysical Journal International* 177(3), pages 1121–1139. DOI: 10.1111/j.1365-246X.2009.04114.x.

Kuster, G. T. and M. N. Toksöz (1974). "Velocity and attenuation of seismic waves in two-phase media: Part I. theoretical formulations". *Geophysics* 39(5), pages 587–606. DOI: 10.1190/1.1440450.

Lemmon, E. W., M. O. McLinden, and D. G. Friend (2005). "Thermophysical properties of fluid systems". *In: Lindstrom, P.J., Mallard, W.G. (eds.), NIST Chemistry Webbook 69, NIST Standard Reference Database, Gaithersburg, MD, USA, http://webbook.nist.gov/chemistry/*. DOI: 10.18434/T4D303.

Lin, G., F. Amelung, P. M. Shearer, and P. G. Okubo (2015). "Location and size of the shallow magma reservoir beneath Kilauea caldera, constraints from near-source Vp/Vs ratios". *Geophysical Research Letters* 42(20), pages 8349–8357. DOI: 10.1002/2015GL065802.

Lin, G. and B. Wu (2018). "Seismic velocity structure and characteristics of induced seismicity at the Geysers Geothermal Field, eastern California". *Geothermics* 71, pages 225–233. DOI: 10.1016/j.geothermics.2017.10.003.

Londono, J. M. (2010). "Activity and Vp/Vs ratio of volcano-tectonic seismic swarm zones at Nevado del Ruiz volcano, Colombia". *Earth Sciences Research Journal* 14(1), pages 111–124.

Londono, J. M. and H. Kumagai (2018). "4D seismic tomography of Nevado del Ruiz Volcano, Colombia, 2000-2016". *Journal of Volcanology and Geothermal Research* 358, pages 156–168. DOI: 10.1016/j.jvolgeores.2018.02.015.

Lowrie, W. and A. Fichtner (2020). *Fundamentals of geophysics*. 3rd edition. Cambridge university press. ISBN: 9781108685917. DOI: 10.1017/9781108685917.

Markus, U. I., J. Ba, J. M. Carcione, L. Zhang, and M. Pang (2022). "3-D Rock-Physics Templates for the Seismic Prediction of Pore Microstructure in Ultra-Deep Carbonate Reservoirs". *Arabian Journal for Science and Engineering* 47, pages 7309–7323. DOI: 10.1007/s13369-021-06232-z.

Matsumoto, Y., M. Ishikawa, M. Terabayashi, and M. Arima (1986). "Simultaneous measurements of compressional wave and shear wave velocities, Poisson's ratio, and Vp/Vs under deep crustal pressure and temperature conditions: Example of silicified pelitic schist from Ryoke Belt, Southwest Japan". *Island Arc* 19, pages 30–39. DOI: 10.1111/j.1440-1738.2009.00695.x.

Mavko, G., T. Mukerji, and J. Dvorkin (2009). *The rock physics handbook: Tools for seismic analysis of porous media*. Cambridge Univ. Press, New York. DOI: https://doi.org/10.1017/CBO9780511626753.

Mayer, K., B. Scheu, C. Montanaro, T. I. Yilmaz, R. Isaia, D. Aßbichler, and D. B. Dingwell (2016). "Hydrothermal alteration of surficial rocks at Solfatara (Campi Flegrei): Petrophysical properties and implications for phreatic eruption processes". *Journal of Volcanology and Geothermal Research* 320, pages 128–143. DOI: 10.1016/j.jvolgeores.2016.04.020.

Miller, P. K., D. M. Saffer, G. A. Abers, D. J. Shillington, A. Bécel, J. Li, and C. Bate (2021). "P- and S-wave velocities of exhumed metasediments from the Alaskan subduction zone: Implications for the in-situ conditions along the megathrust". *Geophysical Research Letters* 48(e2021GL094511). DOI: 10.1029/2021GL094511.

Monsalve, M. L., G. I. Rodriguez, R. A. Mendez, and N. F. Bernal (1998). "Geology of the Well Nereidas 1, Nevado Del Ruiz Volcano, Colombia". *Geothermal Resources Council Transactions* 22, pages 263–267. DOI: 10.32685/pub.esp.38.2019.07.

Moos, D. and M. D. Zoback (1983). "In Situ studies of velocity in fractured crystalline rocks". *Journal of Geophysical Research: Solid Earth* 88(B3), pages 2345–2358. DOI: 10.1029/JB088iB03p02345.

Mordensky, S. P., M. J. Heap, B. M. Kennedy, H. A. Gilg, M. C. Villeneuve, J. I. Farquharson, and D. M. Gravley (2019). "Influence of alteration on the mechanical behaviour and failure mode of andesite: implications for shallow seismicity and volcano monitoring". *Bulletin of Volcanology* 81(44), pages 1–12. DOI: 10.1007/s00445-019-1306-9.

Mordensky, S. P., M. C. Villeneuve, B. Kennedy, M. J. Heap, D. M. Gravley, J. I. Farquharson, and T. Reuschlé (2018). "Physical and mechanical property relationships of a shallow intrusion and volcanic host rock, Pinnacle Ridge, Mt. Ruapehu, New Zealand". *Journal of Volcanology and Geothermal Research* 359, pages 1–20. DOI: 10.1016/j.jvolgeores.2018.05.020.

Moreno, D., J. Lopez-Sanchez, D. Blessent, and J. Raymond (2018). "Fault characterization and heat-transfer modeling to the Northwest of Nevado del Ruiz Volcano". *Journal of South American Earth Sciences* 88, pages 50–63. DOI: 10.1016/j.jsames.2018.08.008.

Muksin, U., K. Bauer, and C. Haberland (2013). "Seismic Vp and Vp/Vs structure of the geothermal area around Tarutung (North Sumatra, Indonesia) derived from local earthquake tomography". *Journal of Volcanology and Geothermal Research* 260, pages 27–42. DOI: 10.1016/j.jvolgeores.2013.04.012.

Murphy, M. D., R. S. J. Sparks, J. Barclay, M. R. Carroll, and T. S. Brewer (2000). "Remobilization of andesite magma by intrusion of mafic magma at the Soufriere Hills volcano, Montserrat, West Indies". *Journal of Petrology* 4(1), pages 21–42. DOI: 10.1093/petrology/41.1.21.

Nakajima, J., T. Matsuzawa, A. Hasegawa, and D. Zhao (2001a). "Seismic imaging of arc magma and fluids under the central part of northeastern Japan". *Tectonophysics* 341(1–4), pages 1–17. DOI: 10.1016/S0040-1951(01)00181-0.

– (2001b). "Three–dimensional structure of Vp, Vs. and Vp/Vs beneath northeastern Japan: Implications for arc magmatism and fluids". *Journal of Geophysical Research: Solid Earth* 106(B10), pages 7505–7516. DOI: 10.1029/2000JB000008.

Nara, Y., P. G. Meredith, T. Yoneda, and K. Kaneko (2011). "Influence of macro-fractures and micro-fractures on permeability and elastic wave velocities in basalt at elevated pressure". *Tectonophysics* 503(1-2), pages 52–59. DOI: 10.1016/j.tecto.2010.09.027.

O'Connell, R. J. and B. Budiansky (1974). "Seismic velocities in dry and saturated cracked solids". *Journal of geophysical Research* 79(35), pages 5412–5426. DOI: 10.1029/JB079i035p05412.

Patanè, D., G. Barberi, O. Cocina, P. D. Gori, and C. Chiarabba (2006). "Time-resolved seismic tomography detects magma intrusions at Mount Etna". *Science* 313(5788), pages 821–823. DOI: 10.1126/science.1127724.

Peacock, S. M., N. I. Christensen, M. G. Bostock, and P. Audet (2011). "High pore pressures and porosity at 35 km depth in the Cascadia subduction zone". *Geology* 39(5), pages 471–474. DOI: 10.1130/G31649.1.

Pimienta, L., A. Schubnel, M. Violay, J. Fortin, Y. Guéguen, and H. Lyon-Caen (2018). "Anomalous Vp/Vs ratios at seismic frequencies might evidence highly damaged rocks in subduction zones". *Geophysical Research Letters* 45(22), pages 12210–12217. DOI: 10.1029/2018GL080132.

Pola, A., G. Crosta, N. Fusi, V. Barberini, and G. Norini (2012). "Influence of alteration on physical properties of volcanic rocks". *Tectonophysics* 566–567, pages 67–86. DOI: 10.1016/j.tecto.2012.07.017.

Pola, A., G. B. Crosta, N. Fusi, and R. Castellanza (2014). "General characterization of the mechanical behaviour of different volcanic rocks with respect to alteration". *Engineering Geology* 169, pages 1–13. DOI: 10.1016/j.enggeo.2013.11.011.

Rabbel, W., T. Jusri, D. Köhn, H. B. Motra, J. Niederau, L. Schreiter, M. Thorwart, and F. Wuttke (2017). "Seismic velocity uncertainties and their effect on geothermal predictions: A case Study". *Energy Procedia* 125, pages 283–290. DOI: 10.1016/j.egypro.2017.08.178.

Rejeki, S., J. Hadi, and I. Suhayati (2005). "Porosity Study for Detail Reservoir Characterization in Darajat Geothermal Field, West Java, Indonesia". *Proceedings World Geothermal Congress*, pages 1–7.

Romero-Jr, A. E., T. V. McEvilly, E. L. Majer, and D. Vasco (1995). "Characterization of the geothermal system beneath the Northwest Geysers steam field, California, from seismicity and velocity patterns". *Geothermics* 24(4), pages 471–487. DOI: 10.1016/0375-6505(95)00003-9.

Savage, M. K., A. Wessel, N. A. Teanby, and A. W. Hurst (2010). "Automatic measurement of shear wave splitting and applications to time varying anisotropy at Mount Ruapehu volcano, New Zealand". *Journal of Geophysical Research: Solid Earth* 115(B12), pages 1–17. DOI: 10.1029/2010JB007722.

Saxena, V., K. Krief, and L. Adam (2018). *Handbook of borehole acoustics and rock physics for reservoir characterization*. Elsevier. DOI: https://doi.org/10.1016/C2016-0-03411-3.

Schmitt, D. R. (2015). "Geophysical Properties of the Near Surface Earth: Seismic Properties". *Treatise on Geophysics*. Edited by G. Schubert. 2nd edition. Volume 11. Elsevier, pages 43–87. ISBN: 978-0-444-53803-1.

Schulze, D. G. (2005). "Clay minerals". *Encyclopedia of Soils in the Environment, Elsevier*. Edited by D. Hillel, pages 246–254. ISBN: 978-0-12-348530-4. DOI: 10.1016/B0-12-348530-4/00189-2.

Simpson, J., K. van Wijk, L. Adam, and C. Smith (2019). "Laser ultrasonic measurements to estimate the elastic properties of rock samples under in situ conditions". *Review of Scientific Instruments* 90(114503), pages 1–8. DOI: 10.1063/1.5120078.

Siratovich, P. A., M. J. Heap, M. C. Villenueve, J. W. Cole, and T. Reuschlé (2014). "Physical property relationships of the Rotokawa Andesite, a significant geothermal reservoir rock in the Taupo Volcanic Zone, New Zealand". *Geothermal Energy* 2(10). DOI: 10.1186/s40517-014-0010-4.

Song, T.-R. A. and Y. Kim (2012). "Localized seismic anisotropy associated with long-term slow-slip events beneath southern Mexico". *Geophysical Research Letters* 39(9), pages 1–6. DOI: 10.1029/2012GL051324.

Spencer-Jr, J. W. and A. M. Nur (1976). "The effects of pressure, temperature and pore water on velocities in westerly granite". *Journal of Geophysical Research* 81(5), pages 899–904. DOI: 10.1029/JB081i005p00899.

Tapias, J. G., N. E. M. Ramírez, M. F. A. Meléndez, F. A. A. Gutiérrez, C. A. M. Montoya, and H. Diederix (2017). "Geological map of colombia 2015". *Episodes* 40(3), pages 201–212. DOI: 10.18814/epiiugs/2017/v40i3/017023.

Tatham, R. H. (1982). "Vp/Vs and lithology". *Geophysics* 74(3), pages 336–344. DOI: 10.1190/1.1441339.

Timur, A. (1977). "Temperature dependence of compressional and shear wave velocities in rocks". *Geophysics* 42(5), pages 950–956. DOI: 10.1190/1.1440774.

Vargas, C. A., I. Koulakov, C. Jaupart, V. Gladkov, E. Gomez, S. E. Khrepy, and N. Al-Arifi (2017). "Breathing of the Nevado del Ruiz Volcano reservoir, Colombia, inferred from repeated seismic tomography". *Scientific Reports* 7(46094), pages 7505–7516. DOI: 10.1038/srep46094.

Vélez, M. I., D. Blessent, S. Córdoba, J. López-Sánchez, J. Raymond, and E. Parra-Palacio (2018). "Geothermal potential assessment of the Nevado del Ruiz volcano based on rock thermal conductivity measurements and risk analysis correction". *Journal of South American Earth Sciences* 81, pages 153–164. DOI: 10.1016/j.jsames.2017.11.011.

Walsh, J. B. (1965). "The effect of cracks on the compressibility of rock". *Journal of Geophysical Research* 70(2), pages 381–389. DOI: 10.1029/JZ070i002p00381.

Wang, Q., S. Ji, M. H. Salisbury, B. Xia, M. Pan, and Z. Xu (2005). "Pressure dependence and anisotropy of P-wave velocities in ultrahigh-pressure metamorphic rocks from the Dabie–Sulu orogenic belt (China): Implications for seismic properties of subducted slabs and origin of mantle reflections". *Tectonophysics* 398(1–2), pages 67–99. DOI: 10.1016/j.tecto.2004.12.001.

Wang, X. Q., A. Schubnel, J. Fortin, E. C. David, Y. Guéguen, and H. K. Ge (2012). "High Vp/Vs ratio: Saturated cracks or anisotropy effects?" *Geophysical Research Letters* 36(11), pages 1–6. DOI: 10.1029/2012GL051742.

Wang, Z. ( (2001). "Fundamentals of seismic rock physics". *Geophysics* 66(2), pages 398–412. DOI: 10.1190/1.1444931.

Wang, Z., R. Wang, F. Wang, H. Qiu, and T. Li (2015). "Experiment study of pore structure effects on velocities in synthetic carbonate rocks". *Geophysics* 80(3), pages D207–D219. DOI: 10.1190/geo2014-0366.1.

Wilkens, R., G. Simmons, and L. Caruso (2018). "The ratio Vp/Vs as a discriminant of composition for siliceous limestones". *Exploration Geophysics* 49(11), pages 1850–1860. DOI: 10.1071/EG984263b.

Wilson, M. J. (2004). "Weathering of the primary rock-forming minerals: processes, products and rates". *Clay Minerals* 39, pages 233–266. DOI: 10.1180/0009855043930133.

Zhu, H. (2018). "High Vp/Vs ratio in the crust and uppermost mantle beneath volcanoes in the Central and Eastern Anatolia". *Geophysical Journal International* 214(3), pages 2151–2163. DOI: 10.1093/gji/ggy253.